International Journal of Geographical Information Science
Vol. 00, No. 00, Month 2010, 1–26

PREPRINT

Numerical Experiments with Cooperating Multiple Quadratic Snakes for Road Extraction

Y. NAKAGURO*†, S. S. MAKHANOV†, and M. N. DAILEY‡

†Sirindhorn International Institute of Technology, Thammasat University, Pathumthani, Thailand
‡Computer Science and Information Management, Asian Institute of Technology, Pathumthani, Thailand

(*May 2010*)

Higher-order active contours or snakes show much promise for extraction of complex objects from noisy imagery. These models provide an elegant mathematical framework for specifying the desired properties of target objects via energy functionals that can be minimized with standard optimization techniques. However, techniques to allow quadratic snakes to change topology during segmentation have not been fully exploited. Additionally, external forces for improving convergence of quadratic snakes have similarly yet to be explored. In this paper, we propose a model that allows multiple quadratic snakes to split, merge and disappear. Although the separate components of our approach have been introduced elsewhere Cohen (1991), Xu and Prince (1997), Rochery *et al.* (2006), this paper is the first comprehensive empirical study of their performance on real-world complex network extraction tasks. We analyze the applicability of the model to road extraction from satellite images that vary in complexity from simple networks to large networks with multiple loops. We also analyze the effects of external forces enhanced by oriented filtering, gradient vector flow fields, and Canny edge detection. In a series of experiments, we found that the multiple cooperating quadratic snake model performs well on complex, noisy images. Our experiments also establish a performance improvement when the proposed quadratic model is coupled with the Canny-based gradient vector flow technique.

Keywords: Higher-order active contours; Road extraction

*Corresponding author. Email: ynakaguro@siit.tu.ac.th

ISSN: 1365-8816 print/ISSN 1362-3087 online

DOI: 10.1080/1365881YYxxxxxxxx
http://www.informaworld.com

1. Introduction

Extracting linear structures such as road, river, and blood vessel networks from images is a challenging problem with many practical applications. Although accurate methods exist for tracking (Geman and Jedynak 1996), it is very difficult to extract complete networks in the presence of noise and distracting features. Existing approaches to fully automatic road extraction include dynamic programming (Fischler *et al.* 1981, Barzohar and Cooper 1996), Markov random fields (Regazzoni *et al.* 1995, Tupin *et al.* 1998), and other techniques (see Auclair-Fortier *et al.* (2000) for a complete overview), but some of the most successful approaches for road segmentations (Fua and Leclerc 1990, Rochery *et al.* 2006), vessel segmentations (Tang and Acton 2004), and online video sequences (Sawano and Okada 2004), so far have been based on active contours or snakes.

Classical active contour models (Kass *et al.* 1987, Cohen 1991, Cohen and Cohen 1993) provide an elegant framework for optimal estimation in image processing; rather than writing an algorithm to extract the object or region of interest, we simply consider an energy functional a minimum of which is achieved at a good solution. Then, given a new image, we use general optimization techniques to find a contour minimizing the energy functional.

The main drawback of the classical parametric active contour model is its lack of topological flexibility. When there are several objects in an image that need to be captured, we require manual initialization of multiple contours or active methods able to "break" contours into multiple pieces (Samadani 1989, Durkovich *et al.* 1995, Ngoi and Jia 1999, Choi *et al.* 2001, McInerney and Terzopoulos 2000, Giraldi *et al.* 2003). Even if we allow contours to split and merge, we encounter the problem that individual snakes can intersect themselves and each other, requiring geometric constraints to prevent intersections (Ivins and Porrill 1995) or explicit detection and handling of intersections (Wong *et al.* 1998, Ngoi and Jia 1999, Ji and Yan 2002). This problem is especially troublesome when nested snakes are initialized inside one another.

So far, level set methods (Sethian 1999) appear to be the most elegant approach to the problems of active contour topological flexibility and self-intersection (Caselles *et al.* 1993, Malladi *et al.* 1995, Rochery *et al.* 2006). Level set methods, which represent a curve implicitly as the zero level set of an evolving hypersurface, allow curves to automatically break or merge. However, level set methods do not readily admit imposition of arbitrary geometric constraints (McInerney and Terzopoulos 2000) or external forces, and they are relatively susceptible to image noise (Xu *et al.* 2000), so methods to obtain the topological flexibility of level set methods within the more mathematically flexible framework of explicit contour representations are still under active research (Delingette and Montagnat 2000, Li *et al.* 2005).

Our network extraction approach is based on Xu and Prince's gradient vector flow (GVF, Xu and Prince 1997), Rochery's quadratic active contours (Rochery *et al.* 2006), and efficient algorithms for splitting, merging, and deleting contours presented in this paper. The model can be easily modified to include other types of the gradient vector flow models such as the generalized gradient vector flow (Xu and Prince 1998a), multi-direction GVF (Tang 2009), etc. Our *quadratic multiple snake model* represents a compromise between geometric snakes' ability to split and merge easily and parametric snakes' flexibility to incorporate arbitrary constraints. We use quadratic constraints (Rochery *et al.* 2006) both to avoid self-intersections and loops and as a means to encourage capture of thin elongated objects such as roads, rivers, canal systems, pipes, and vascular systems. Our split and merge algorithms employ straightforward conditions on the close-

ness of non-adjacent contour points. In the model, separate snakes can repel each other but are still capable of approaching an object from opposite sides. The split and merge algorithms make it possible to extract highly complex networks of roads and other linear structures. The model thus provides the topological adaptability of geometric models without sacrificing the simplicity, efficiency, or flexibility of traditional parametric models.

In this paper, we provide the mathematical motivation for the model and perform a series of numerical experiments to evaluate the effectiveness of the approach on real satellite data. We manipulate three factors:

- **Noise level**: we prepare noised images by adding varying levels of Gaussian noise to an original image containing a clear road network, and evaluate the tolerance of the proposed approach against noise.
- **Type of external force**: we compare two types of the external force for contour evolution: one using Xu and Prince's Gradient Vector Flow (Xu and Prince 1997) applied directly to the image gradient, and one using a GVF applied to the gradient of a binary image resulting from oriented filtering combined with Canny edge detection.
- **Model order**: we contrast conventional linear snakes against quadratic snakes (Rochery *et al.* 2006) that allow contour points with opposite normals to repel each other unless they are aligned with opposite sides of the same ridge edge.

Although the separate components of our approach have been introduced elsewhere (Cohen 1991, Xu and Prince 1997, Rochery *et al.* 2006), this paper is the first comprehensive empirical study of their performance on real-world complex network extraction tasks. For each active contour model and road network extraction task, we perform a detailed analysis of the model's precision and convergence time. Our main finding is that the multiple cooperating quadratic snake model allowing splitting and merging of contours performs well on complex, noisy images with road networks of multiple scales.

2. Method

2.1. *Quadratic snake model*

This section provides a brief overview of the quadratic snake proposed by Rochery *et al.* (2006). An *active contour* or *snake* is parametrically defined as

$$\boldsymbol{\gamma}(p) = \left[x(p)\ y(p)\right]^T, \tag{1}$$

where p is the curvilinear abscissa of the contour and the vector $\left[x(p)\ y(p)\right]^T$ defines the Cartesian coordinates of the point $\boldsymbol{\gamma}(p)$.

The energy functional is given by

$$E_s(\boldsymbol{\gamma}) = E_g(\boldsymbol{\gamma}) + \lambda E_i(\boldsymbol{\gamma}), \tag{2}$$

where $E_g(\boldsymbol{\gamma})$ is the *geometric energy* and $E_i(\boldsymbol{\gamma})$ is the *image energy* of the contour $\boldsymbol{\gamma}$. λ is a free parameter determining the relative importance of the two terms.

To apply the method to road extraction, we define the geometric energy functional to

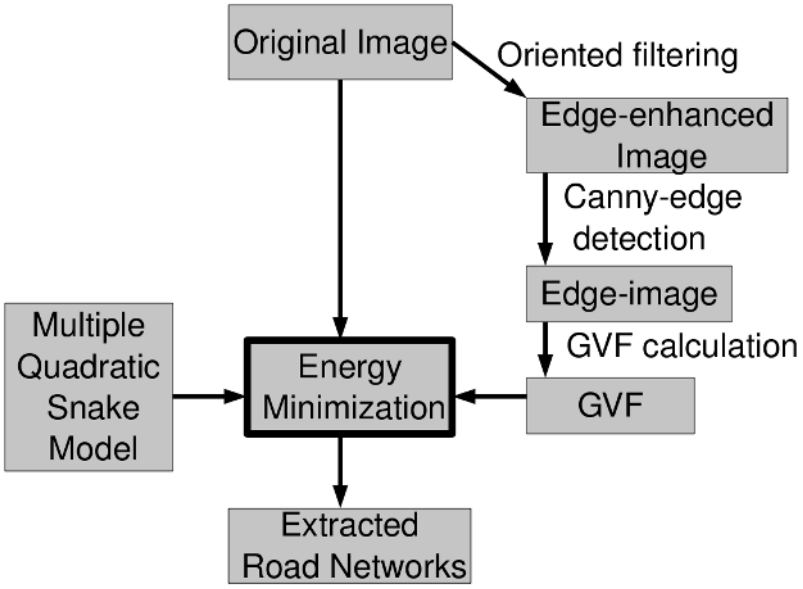

Figure 1. Overview of the multiple quadratic snake system for road extraction.

be

$$E_g(\boldsymbol{\gamma}) = L(\boldsymbol{\gamma}) + \alpha A(\boldsymbol{\gamma}) - \frac{\beta}{2} \iint \boldsymbol{t}(p) \cdot \boldsymbol{t}(p') \; \Psi\left(\|\boldsymbol{\gamma}(p) - \boldsymbol{\gamma}(p')\|\right) \; dp \; dp', \tag{3}$$

where $L(\boldsymbol{\gamma})$ is the Euclidean length of $\boldsymbol{\gamma}$, $A(\boldsymbol{\gamma})$ is the area enclosed by $\boldsymbol{\gamma}$, $\boldsymbol{t}(p)$ is the unit-length tangent to $\boldsymbol{\gamma}$ at point p, and $\Psi(z)$, given the distance z between two points on the contour, is used to weight the interaction between those two points (see below). α and β are constants weighting the relative importance of the terms. The functional is a combination of two linear, Euclidean invariant terms: the area and the length. The length term acts as a regularizer, whereas the area term controls the expansion of the region. For positive β, $E_g(\boldsymbol{\gamma})$ is minimized by contours with short length and parallel tangents. If α is positive, contours with small enclosed area are favored; if it is negative, contours with large enclosed area are favored.

The third quadratic (also Euclidean invariant) term is responsible for interactions between points on the snake. The interaction function $\Psi(\cdot)$ is a smooth function expressing the radius of the region in which parallel tangents should be encouraged and anti-parallel tangents should be discouraged:

$$\Psi(z) = \begin{cases} 1 & \text{if } z < d - \epsilon, \\ 0 & \text{if } z > d + \epsilon, \\ \frac{1}{2}\left(1 - \frac{z-d}{\epsilon} - \frac{1}{\pi}\sin\pi\frac{z-d}{\epsilon}\right) & \text{otherwise.} \end{cases} \tag{4}$$

In application to road extraction, d is the expected road width and ϵ expresses the expected variability in road width. During snake evolution, weighting by $\Psi(z)$ in equation (3) discourages two points with anti-parallel tangents (the opposite sides of a putative road) from coming closer than distance d from each other.

The image energy functional $E_i(\boldsymbol{\gamma})$ is defined as

$$\begin{aligned} E_i(\boldsymbol{\gamma}) = & \int \boldsymbol{n}(p) \cdot \nabla I(\boldsymbol{\gamma}(p))\ dp \\ & - \iint \boldsymbol{t}(p) \cdot \boldsymbol{t}(p')\ \nabla I(\boldsymbol{\gamma}(p)) \cdot \nabla I(\boldsymbol{\gamma}(p'))\ \Psi(\|\boldsymbol{\gamma}(p) - \boldsymbol{\gamma}(p')\|)\ dp\ dp', \end{aligned} \tag{5}$$

where $I : \Omega \to [0, 255]$ is an image and $\nabla I(\boldsymbol{\gamma}(p))$ is the gradient of I evaluated at $\boldsymbol{\gamma}(p)$.

The first (linear) term favors anti-parallel normal and gradient vectors, encouraging counterclockwise snakes to shrink around or clockwise snakes to expand to enclose dark regions surrounded by light roads.[1] The second (quadratic) term favors nearby point pairs with two different configurations, one with parallel tangents and parallel gradients and the other with anti-parallel tangents and anti-parallel gradients.

To find a curve $\boldsymbol{\gamma}$ minimizing $E_s(\boldsymbol{\gamma})$, one obtains the Euler equations using the calculus of variations. Introducing the gradient descent method and ignoring flow in the direction tangent to $\boldsymbol{\gamma}$, one obtains

$$\begin{aligned} \boldsymbol{n}(p) \cdot \frac{\partial \boldsymbol{\gamma}}{\partial t} = & -\kappa(p) - \alpha - \lambda \nabla^2 I(\boldsymbol{\gamma}(p)) \\ & + \beta \int \boldsymbol{r}\left(\boldsymbol{\gamma}(p), \boldsymbol{\gamma}(p')\right) \cdot \boldsymbol{n}(p')\ \ \Psi'\left(\|\boldsymbol{\gamma}(p) - \boldsymbol{\gamma}(p')\|\right) dp' \\ & + 2\lambda \int \boldsymbol{r}\left(\boldsymbol{\gamma}(p), \boldsymbol{\gamma}(p')\right) \cdot \boldsymbol{n}(p')\ \ \left(\nabla I(\boldsymbol{\gamma}(p)) \cdot \nabla I(\boldsymbol{\gamma}(p'))\right)\ \ \Psi'\left(\|\boldsymbol{\gamma}(p) - \boldsymbol{\gamma}(p')\|\right) dp' \\ & + 2\lambda \int \nabla I(\boldsymbol{\gamma}(p')) \cdot \left(\nabla \nabla I(\boldsymbol{\gamma}(p)) \boldsymbol{n}(p')\right)\ \ \Psi(\|\boldsymbol{\gamma}(p) - \boldsymbol{\gamma}(p')\|)\ dp'. \end{aligned} \tag{6}$$

In the equation, $\kappa(p)$ is the curvature of $\boldsymbol{\gamma}$ at $\boldsymbol{\gamma}(p)$ and $\nabla^2 I(\boldsymbol{\gamma}(p))$ is the Laplacian of I evaluated at $\boldsymbol{\gamma}(p)$.

$$\boldsymbol{r}\left(\boldsymbol{\gamma}(p), \boldsymbol{\gamma}(p')\right) = \frac{\boldsymbol{\gamma}(p) - \boldsymbol{\gamma}(p')}{\|\boldsymbol{\gamma}(p) - \boldsymbol{\gamma}(p')\|}$$

is the unit vector pointing from point $\boldsymbol{\gamma}(p)$ towards $\boldsymbol{\gamma}(p')$. $\nabla \nabla I(\boldsymbol{\gamma}(p))$ is the 2×2 Hessian of I evaluated at $\boldsymbol{\gamma}(p)$. α, β, and λ are free parameters that need to be determined experimentally. d and ϵ are specified a priori according to the desired road width.

2.2. *GVF external force*

The term $\alpha A(\boldsymbol{\gamma})$ in equation (3) leads to the constant term $-\alpha$ in equation (6). This term provides a force similar to the "balloon force" introduced by Cohen and Cohen (1993). It increases the capture region around objects, but its effect is uniform throughout the image. This makes it difficult to specify a value for α that is appropriate in all regions of the image.

[1] For dark roads on a light background, we simply negate the terms involving the image. In the rest of the paper, we assume light roads on a dark background.

Xu and Prince (Xu and Prince 1997, 1998b) have proposed to use, rather than a global balloon force, a smooth, diffuse gradient field as a local external force with the traditional linear snake. They find that this technique, gradient vector flow (GVF), improves the traditional snake's convergence to a minimum energy configuration.

We propose the use of GVF with quadratic road extraction snakes (see Figure1).

2.2.1. GVF

The GVF is a vector field $\boldsymbol{V}(x,y) = \left[u(x,y)\ v(x,y)\right]^T$ minimizing the energy functional

$$E(\boldsymbol{V}) = \int_\Omega \mu \left(\left\| \frac{\partial \boldsymbol{V}}{\partial x} \right\|^2 + \left\| \frac{\partial \boldsymbol{V}}{\partial y} \right\|^2 \right) + \|\nabla \widetilde{I}\|^2 \|\boldsymbol{V} - \nabla \widetilde{I}\|^2 \, dx \, dy, \tag{7}$$

where $\widetilde{I}$ is a preprocessed version of image I, typically an edge image of some kind. The first term inside the integral encourages a smooth vector field whereas the second term encourages fidelity to $\nabla \widetilde{I}$. μ is a free parameter controlling the relative importance of the two terms. Minimizing functional (7) leads to the Euler equation given by

$$\mu \nabla^2 \boldsymbol{V} - (\boldsymbol{V} - \nabla \widetilde{I}) \|\nabla \widetilde{I}\|^2 = 0. \tag{8}$$

Equation (8) is then solved numerically by iterations. Furthermore, replacing μ in (8) by two weighting functions depending on $\nabla \widetilde{I}$ to control the relative importance of the two terms $\nabla^2 \boldsymbol{V}$ and $(\boldsymbol{V} - \nabla \widetilde{I}) \|\nabla \widetilde{I}\|^2$ leads to the so–called generalized version of the GVF (Xu and Prince 1998a).

We obtain $\widetilde{I}$ using oriented filtering and Canny edge detection combined with elongated Laplacian of Gaussian filters that emphasize road-like structures, deemphasize non-road-like structures, and, to a certain extent, fill in short gaps where a road has low contrast with the background. The resulting binary Canny image only includes information about road-like edges that have survived sharpening by the oriented filters. The GVF field on top of the sharpened edge image points toward the road-like edges from a long distance, and, during snake evolution, it pushes the snake in an appropriate direction. This speeds evolution and makes it easier to find suitable parameters to obtain fast convergence.

2.2.2. Oriented filtering

Using oriented filters for contour detection, contour completion, and restoration of edges corrupted by noise is a recurring idea in image processing and computer vision (see, e.g., Knutsson *et al.* (1983), Perona and Malik (1990), Freeman and Adelson (1991), Steger (1998), Konishi *et al.* (2003)). The oriented filters most frequently used are 2D Gabor filters (Daugman 1985) and directional Laplacian of Gaussian (LoG) filters. Gabor filters are thought to be good models of the response of simple cells in primary visual cortex (Jones and Palmer 1987). When paired symmetric (even) and antisymmetric (odd) oriented filter responses are combined by summing their squares, they are thought to be good models of the response of complex cells in primary visual cortex (Heitger *et al.* 1992). Perona and Malik (1990) advocate these paired "energy filters" for their ability to detect not only step edges but also ridge edges at specific scales.

The ability of Gabor filters and LoG filters to detect ridge edges makes them ideal for identifying roads in satellite imagery. Our oriented filtering method is the same as that of Rochery et al. (Rochery *et al.* 2006). We use the linear response of elongated LoG filters tuned to detect roads at 8 orientations then (for bright roads with dark surround) take the minimum response over the 8 orientations. An example is shown in figure 2.

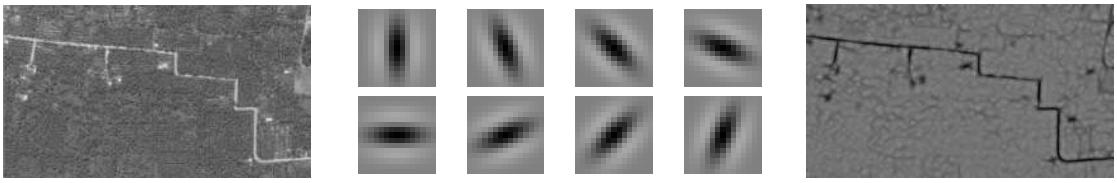

(a) (b) (c)

Figure 2. Oriented filtering procedure for enhancing road contrast. (a) Original image. (b) Laplacian–of–Gaussian filters at 8 orientions, with horizontal standard deviation 1.0 and vertical standard deviation 3.0. (c) Pixelwise convolution minimum over all 8 orientations.

Our convolution and minimum response selection procedure responds well to long straight edges having the effect of emphasizing road-like gradients, deemphasizing non-road-like gradients, and, to a certain extent, filling in short gaps where a road has low contrast with the background.

2.2.3. Obtaining the GVF field

After oriented filtering, we obtain the Canny edge image $\widetilde{I}$ from the edge-enhanced image obtained from oriented filtering. This is the input to the GVF relaxation procedure (Xu and Prince 1997). We precalculate $\boldsymbol{V}$ before snake evolution begins, then, similar to Xu and Prince, during evolution, for each point $\boldsymbol{\gamma}(p)$, we add the force $\lambda_{GVF}\ \boldsymbol{n}(p) \cdot \boldsymbol{V}(\boldsymbol{\gamma}(p))$ directly to the update equation (6). λ_{GVF} is a weight trading off the importance of the GVF force against the other forces in equation (6).

Clearly, this encourages the snake to snap to the road edge contours, where ideally $\|\boldsymbol{V}(\boldsymbol{\gamma}(p))\| = 0$.

Our experimental results show that this approach, combining the advantages of the GVF's extended capture range and the quadratic snake's flexibility, improves the snake's convergence to configurations that accurately segment road-like structures.

2.3. *Family of quadratic snakes*

A single quadratic snake is unable to extract enclosed regions and multiple disconnected networks in an image. We address this limitation by introducing a *family* of cooperating snakes that are able to split, merge, and disappear as necessary.

In our formulation, due to the curvature term $\kappa(p)$ and the area constant α in equation (6), specifying the points on $\boldsymbol{\gamma}$ in a counterclockwise direction creates a *shrinking snake* and specifying the points on $\boldsymbol{\gamma}$ in a clockwise direction creates a *growing snake*.

An enclosed region (loop or a grid cell) can be extracted effectively by initializing two snakes, one shrinking snake covering the whole road network and another growing snake inside the enclosed region.

2.3.1. Splitting a snake

We split a snake into two snakes whenever two of its arms are squeezed too close together, i.e., when the distance between two snake points is less than d^{split} and those two points are at least k snake points from each other in both directions of traversal around the contour (see Figure3(a) for an example). d^{split} should be less than 2η, where η is the maximum step size.

2.3.2. Merging two snakes

The merging algorithm selects points having high curvature and merges two snakes when 1) two selected points are closer than a prescribed minimal merging distance d^{merge}, 2) the traversal direction (clockwise or counterclockwise) of the two snakes is the same, and 3) the tangents at the two high curvature points are nearly antiparallel. Figure 3(b) shows an example of two snakes merging each other. High curvature points are those with $\kappa_{\boldsymbol{\gamma}(p)} > 0.6\kappa_{\boldsymbol{\gamma}}^{\max}$, where $\kappa_{\boldsymbol{\gamma}}^{\max}$ is the maximum curvature for any point on $\boldsymbol{\gamma}$. When these conditions are satisfied, the two snakes are combined into a single snake by deleting the high curvature points and merging at the holes.

Limiting the merge decision to high curvature points ensures that merging only occurs if two snakes have semi-circular tips of their arms facing each other. It might seem that merging at low curvature points should also be permitted. However, as already explained, snakes normally repel each other due to the quadratic term in the internal energy (equation (3)). Consequently, low curvature segments can approach each other when high-gradient features allow the external energy to overcome the geometric energy. When this occurs for low curvature segments, the two snakes are most likely positioned on different sides of a road and merging should not be allowed. There are several other (rare) cases when snakes face each other at low curvature parts. However they should not be merged in those cases either.

Considering only the high curvature points also saves computational costs. In particular, the merging procedure requires computation of the angle between tangents only for the selected points. The number of those points usually does not exceed 10% of the total number of points.

The conditions that the traversal direction of two snakes should be the same and that the tangents at the two high curvature points should be antiparallel reflect the fact that in our system, nested snakes form a tree structure. We initialize all the snakes at the first level with the same direction of traversal. The second level has the opposite direction of traversal and so on. When two snakes from the same level merge, we assign the resulting snake the same direction. Snakes from two consecutive levels do not merge. Growing and shrinking behavior is controlled by the area constant (α) and the weight on the geometric energy (β).

2.3.3. Deleting a snake

A snake $\boldsymbol{\gamma}$ is deleted if it has perimeter less than L^{delete}. Figure 3(c) shows an example of a snake being deleted.

2.4. *Experimental design*

We present four experiments aimed at evaluating the cooperating snake model for road extraction. In Experiment 1, we evaluate the robustness of the model against noise. Beginning with an image containing a clear road network, we progressively add Gaussian noise. The initialization is a single contour along the boundary of each image. In Experiment 2, we evaluate the model on an image containing a road network with many loops, intersections, and distracting structures, shown in Figure 6. This image requires multiple initial contours and user initialization to successfully segment the road network while ignoring the background region surrounded by the road loop. Furthermore, extraction of this road network requires a model capable of splitting at artifacts created by the noise. In Experiment 3, we evaluate the model on an image containing a road network with widely varying widths. Although varying the parameter ϵ accommodates modest width

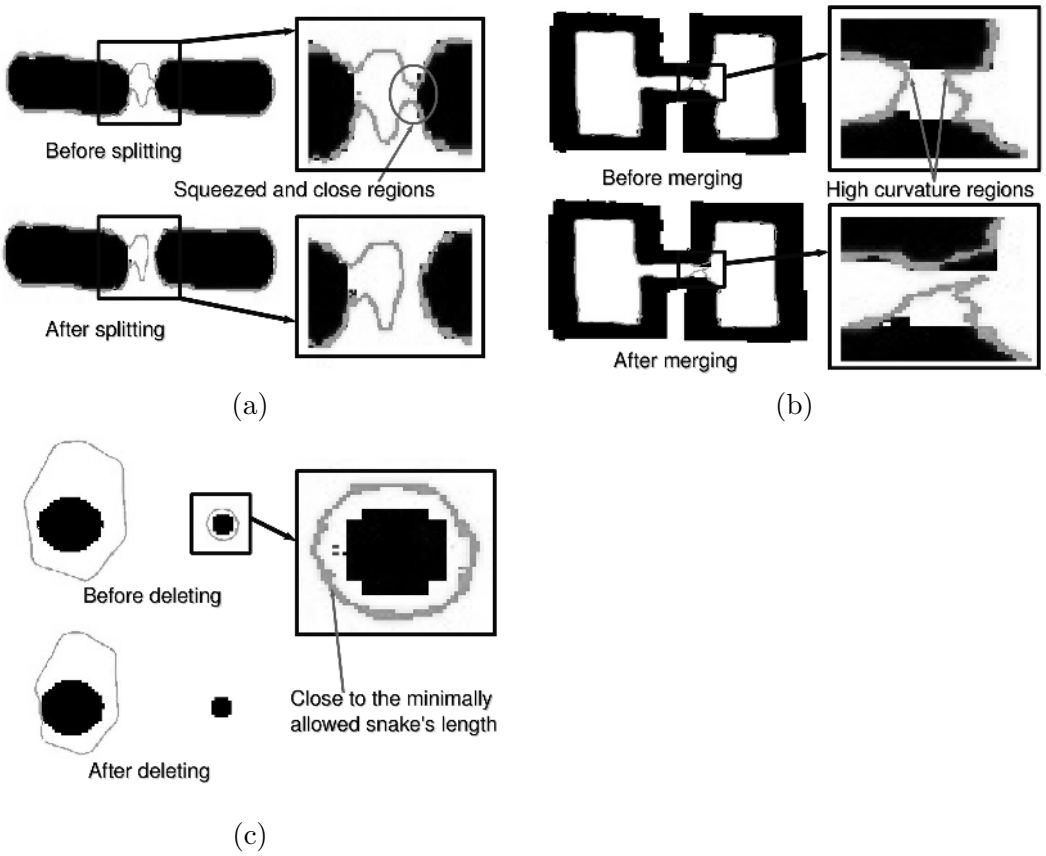

Figure 3. Cooperating snakes. (a) A shrinking snake splits into two snakes and finally captures two distant objects. (b) Two merging snakes. (c) Two shrinking snakes one of which has been deleted after reaching a minimally allowed length.

variations, we need a consistent approach for roads with significantly different scales. Therefore, to extract the entire road network, we independently optimize parameter sets for large-width roads and small-width roads, then we perform extractions using the two different sets of parameters, and then we finally combine the extracted large-width roads and small-width roads. The initialization is the image boundary in the large-width case, and multiple contours along the outlines of roads in the small-width case. Finally, in Experiment 4, we evaluate the spacial scalability of the model on an image containing a large-scale complex road network. We show an initialization with multiple snakes in Figure 11 (b). The images were obtained using Google Earth software.

We manipulate three factors:

- **Noise level**. We add four levels of Gaussian noise (25 dB, 20 dB, 15 dB, and 10 dB) to the original image (see Figure 4 and 5).
- **GVF type**. In the first condition, *PlainGVF*, the GVF is calculated from the result of oriented filtering on image I directly. In the second condition, *CannyGVF*, the GVF is the result of oriented filtering and Canny edge extraction as described in section 2.2.
- **Model order**. In the first condition, *Linear*, we use the simple linear snake model obtained by eliminating the quadratic terms from equations (3) and (5). In the second condition, *Quadratic*, the full interactions in equations (3) and (5) are included.

In Experiment 1, we only manipulate the noise level and use the quadratic snakes with the Canny-based GVF. In Experiments 2, 3, and 4, we only manipulate the GVF type

Table 1. Parameters in Experiment 1.

Condition	σ_x	σ_y	α	β	λ	λ_{GVF}	d	ϵ
Non-noised	2.9	5.4	0.4	0.3	3.0	0.2	2.8	0.75
SNR 25 dB	2.9	5.4	0.4	0.3	3.0	0.2	2.8	0.75
SNR 20 dB	2.9	6.4	0.6	0.3	3.0	0.2	2.8	0.75
SNR 15 dB	3.3	6.6	0.6	0.3	3.0	0.2	2.8	0.75
SNR 10 dB	2.9	6.3	0.4	0.3	3.0	0.2	2.8	0.75

and model order. With 2 levels for each of 2 factors, we have 4 possible manipulations for each of these experiments.

For each manipulation, we hand-tune the free parameters to achieve the best possible results. In oriented filtering, we adjust σ_x and σ_y, the standard deviations of the elongated Gaussian, until we obtain clear road pixels. Generally, setting σ_x to the approximate road width and σ_y to 1.5–10 times larger than σ_x yields reasonable filtering results. Parameters α, β, λ, λ_{GVF}, d, and ϵ are related to the snake evolution model. Larger α facilitates avoidance of noisy spots with high intensity; however, care should be taken not to overwhelm the contribution of the GVF weighted by λ_{GVF}. We adjust β to be large enough to prevent self-intersections in case of quadratic snakes, or set it to zero otherwise. λ should be larger for linear snakes than for quadratic snakes. This forces the linear snake to snap to road edges. Finally, we adjust the road width d and its permissible deviation ϵ until we achieve the best agreement with the ground truth for the test data.

We terminate contour evolution whenever the energy $E_s(\boldsymbol{\gamma})$ fails to decrease for some number of iterations. We measure not only the number of iterations but also the actual computation time. This is because the computational complexities of quadratic snakes and linear snakes is essentially different; $O(N \cdot \log N)$ for quadratic snakes, and $O(N)$ for linear snakes, where N is the total number of active contour points. Note that we have achieved the $O(N \cdot \log N)$ performance for quadratic snakes by optimizing the neighborhood search of contour points.

To evaluate the results, we create ground truth images manually, and we use them to calculate the precision (the proportion of detected pixels that are road pixels according to the ground truth), the recall (the proportion of road pixels that are detected), and F_1 (the harmonic mean of the precision and the recall) for each solution. Along with these pixel-based measures, we introduce the Hausdorff distance, averaged over all contour points, to measure the geometric similarity between the ground truth and extracted road networks.

3. Results

3.1. *Extraction of road networks from noisy images*

In Experiment 1, we demonstrate the robustness of the proposed quadratic method with Canny-based GVF against a practical range of noise. We observe from Table 2 that the proposed model performs well up to the 15 dB noise level. Note, even in the extreme case of 10 dB noise, the snake succeeds in extracting the gross structure of the original road network, shown in Figure 5(d3).

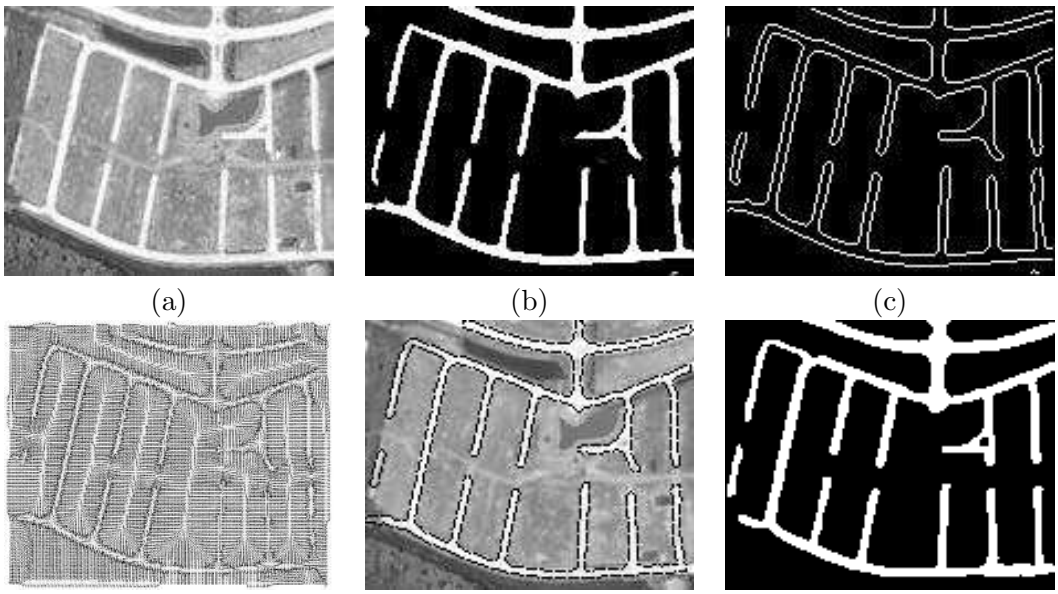

Figure 4. Experiment 1 results for non-noised original image. (a) Non-noised original image, 149x122. (b) Oriented-filtered image. (c) Canny-edges. (d) Canny-based GVF. (e) Road extraction. (f) Ground truth.

Table 2. Extraction results of Experiment 1.

Condition	Iterations	Time (s)	Precision	Recall	F_1	Averaged Hausdorff distance	Graph structure preserved
Non-noised	500	15.3	0.90	0.88	0.89	0.68	Yes
SNR 25 dB	500	14.1	0.92	0.87	0.89	0.69	Yes
SNR 20 dB	700	17.4	0.90	0.83	0.87	0.83	Yes
SNR 15 dB	600	19.9	0.88	0.87	0.87	0.86	Yes
SNR 10 dB	600	11.6	0.93	0.70	0.80	1.66	No

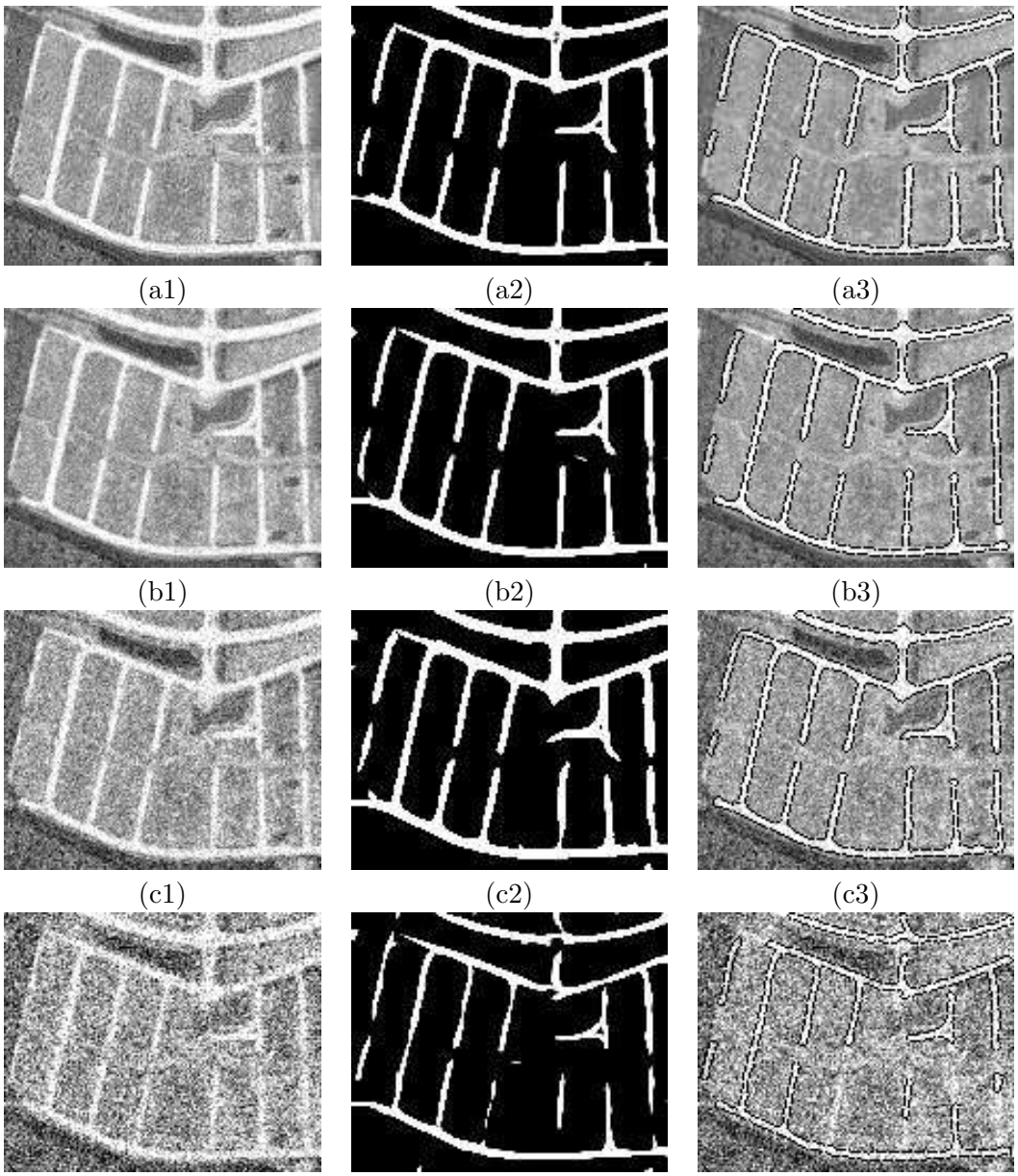

Figure 5. Experiment 1 results for noised images. (a1–a3) SNR = 25 dB. (b1–b3) SNR = 20 dB. (c1–c3) SNR = 15 dB. (d1–d3) SNR = 10 dB. Indices 1,2, and 3 represent an original image, an oriented-filtered image, and extracted road networks, respectively.

3.2. *Extraction of road networks with loops*

The results of Experiment 2 are shown in Figure 7 and Table 4. The results demonstrate the clear superiority of the quadratic model over the linear model. See Table 4. The quadratic interaction model performs much better than the linear model in every case, indicating the importance of the quadratic geometric energy term. The quadratic model is also much better at preserving the road network graph structure. This comes at the cost of a factor of 6 slowdown in runtime performance.

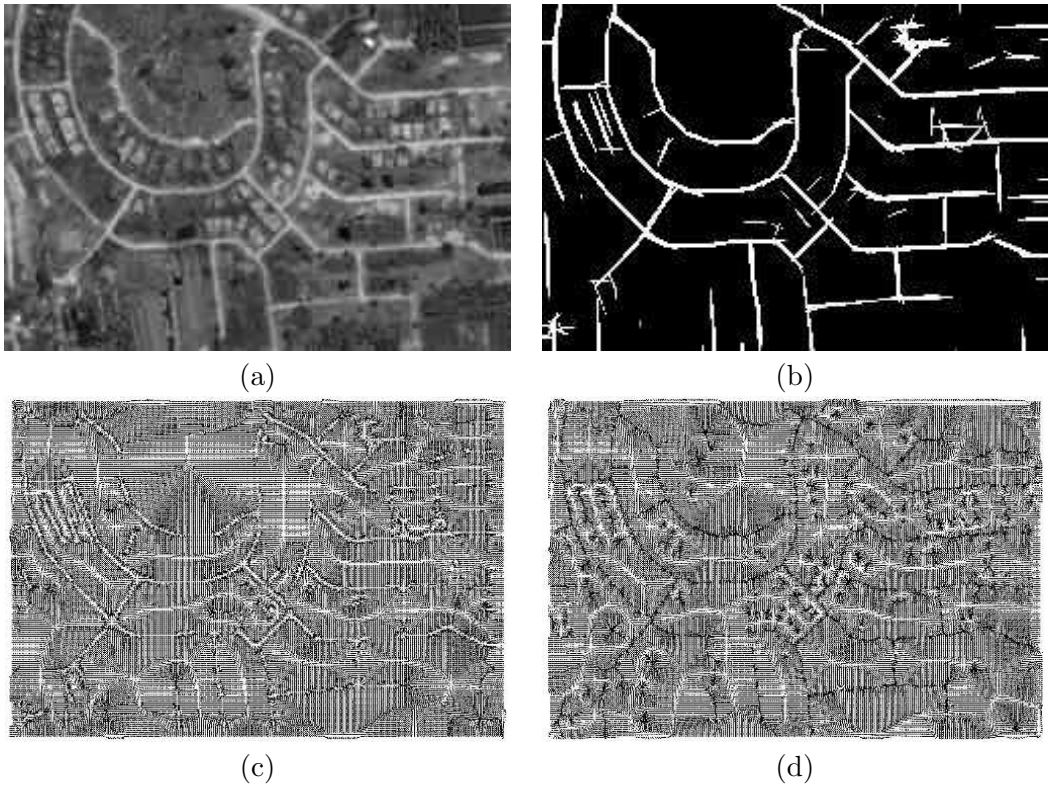

(a) (b)

(c) (d)

Figure 6. Experiment 2. (a) Original image, 250x171. (b) Oriented-filtered image. (c) Canny-based GVF. (d) Plain GVF.

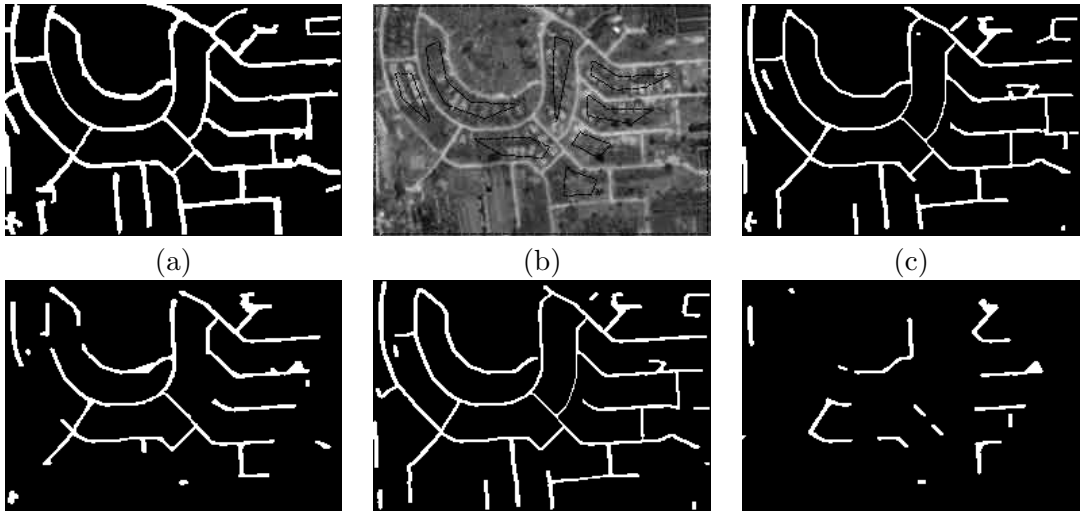

(a) (b) (c)

(d) (e) (f)

Figure 7. Experiment 2. (a) Ground truth. (b) Snake initialization. (c) Extraction with condition CannyGVF–Quadratic. (d) Extraction with condition CannyGVF–Linear. (e) Extraction with condition PlainGVF–Quadratic. (f) Extraction with condition PlainGVF–Linear.

Table 3. Parameters in Experiment 2.

Condition	σ_x	σ_y	α	β	λ	λ_{GVF}	d	ϵ
CannyGVF–Quadratic	1.4	11.2	0.14	0.48	6.4	0.4	1.8	0.70
CannyGVF–Linear	1.4	11.2	0.06	0	60.0	0.4	1.8	0.70
PlainGVF–Quadratic	1.4	11.2	0.14	0.48	6.4	0.4	1.8	0.70
PlainGVF–Linear	1.4	11.2	0.06	0	60.0	0.4	1.8	0.70

Table 4. Extraction results of Experiment 2.

Condition	Iterations	Time (s)	Precision	Recall	F_1	Averaged Hausdorff distance	Graph structure preserved
CannyGVF–Quadratic	760	93.8	0.87	0.60	0.71	1.48	Yes
CannyGVF–Linear	260	15.3	0.87	0.43	0.58	6.16	No
PlainGVF–Quadratic	620	78.1	0.88	0.58	0.70	1.64	Yes
PlainGVF–Linear	280	12.0	0.88	0.18	0.29	14.91	No

3.3. *Extraction of road networks with different widths*

In Experiment 3, examining the results in Figure 9 and Table 6, we see that our approach works well for all manipulations. The quadratic models has a clear advantage over the linear models in correctly capturing thin roads. The bright spots left after oriented filtering in Figure 8(b–c) can be ignored due to the split and delete topological operations. Note that the accuracy of the large–width stage (Table 6) is evaluated against only the large–width part of the network. However, the small–width stage detects the small– and high–width roads leading (formally) to poor accuracy. For instance, the averaged Hausdorff distance in case of CannyGVF–Quadratic–Large is 0.69, whereas the accuracy of CannyGVF–Quadratic–Small is 2.23. However, merging the two results produces good accuracy. The Hausdorff error of CannyGVF–Quadratic–Combined is still 0.69.

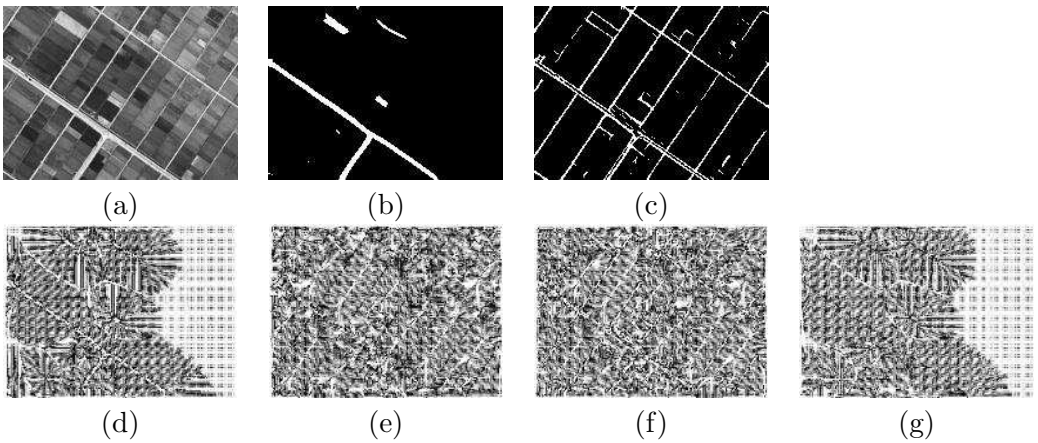

Figure 8. Experiment 3. (a) Original image, 200x148. (b) Oriented-filtered image for large width. (c) Oriented-filtered image for small width. (d) Canny-based GVF for large width. (e) Plain GVF for large width. (f) Canny-based GVF for small width. (g) Plain GVF for small width.

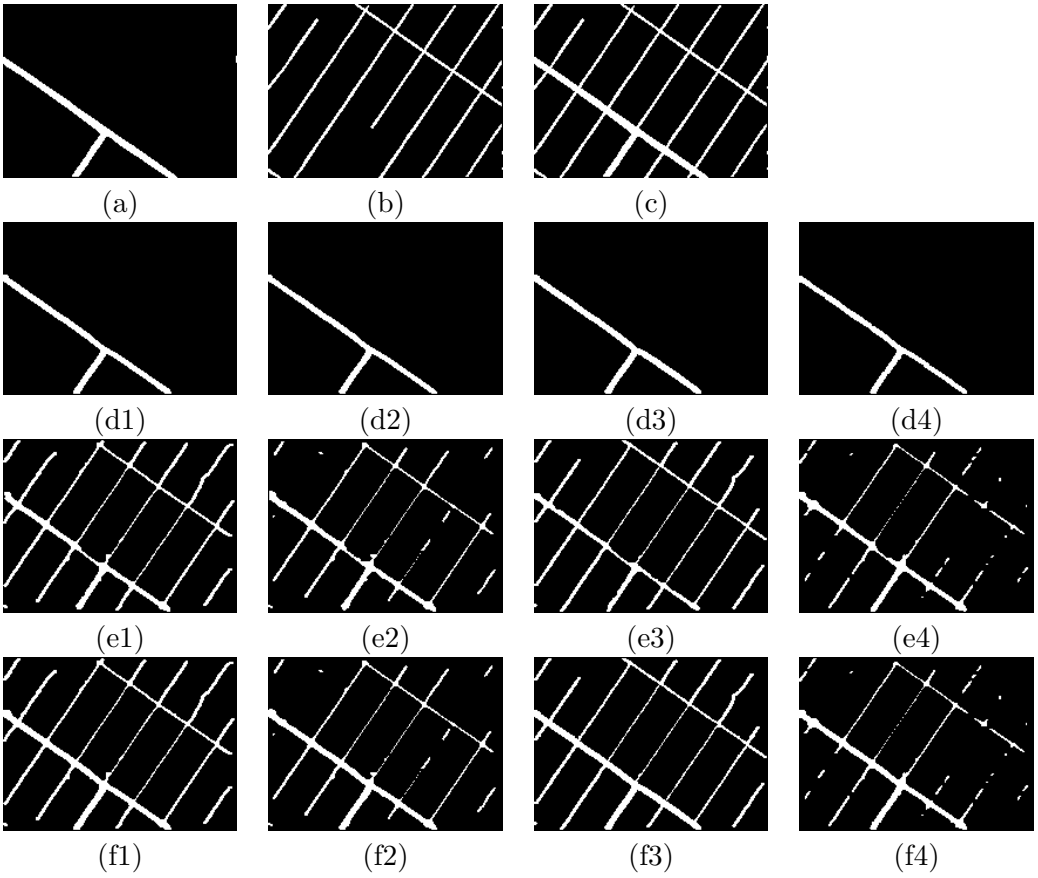

Figure 9. Experiment 3. (a) Ground truth for large width. (b) Ground truth for small width. (c) Ground truth for combined networks. (d1–d4) Extractions for large width. (e1–e4) Extractions for small width. (f1–f4) Extractions for combined networks. Indices 1, 2, 3, and 4 represent conditions CannyGVF–Quadratic, CannyGVF–Linear, PlainGVF–Quadratic, and PlainGVF–Linear, respectively.

Table 5. Parameters in Experiment 3.

Condition	σ_x	σ_y	α	β	λ	λ_{GVF}	d	ϵ
CannyGVF–Quadratic–Large	3.9	9.8	0.4	0.3	3.0	0.2	4.2	0.7
CannyGVF–Linear–Large	3.9	9.8	0.1	0	6.0	0.2	4.2	0.7
PlainGVF–Quadratic–Large	3.9	9.8	0.4	0.3	3.0	0.2	4.2	0.7
PlainGVF–Linear–Large	3.9	9.8	0.1	0	6.0	0.2	4.2	0.7
CannyGVF–Quadratic–Small	0.8	4.4	0.05	0.9	20.0	0.6	2.0	0.25
CannyGVF–Linear–Small	0.8	4.4	0.05	0	40.0	0.6	2.0	0.25
PlainGVF–Quadratic–Small	0.8	4.4	0.05	0.9	20.0	0.6	2.0	0.25
PlainGVF–Linear–Small	0.8	4.4	0.05	0	40.0	0.6	2.0	0.25

Table 6. Extraction results of Experiment 3. (·) is the sum of large-width and small-width experiments.

Condition	Iterations	Time (s)	Precision	Recall	F_1	Averaged Hausdorff distance	Graph structure preserved
CannyGVF–Quadratic–Large	420	5.4	0.97	0.84	0.90	0.69	Yes
CannyGVF–Linear–Large	320	3.8	0.98	0.80	0.88	0.84	Yes
PlainGVF–Quadratic–Large	460	6.0	0.96	0.87	0.91	0.65	Yes
PlainGVF–Linear–Large	280	3.6	0.99	0.77	0.87	0.93	Yes
CannyGVF–Quadratic–Small	40	2.7	0.62	0.75	0.68	2.23	Yes
CannyGVF–Linear–Small	20	1.5	0.56	0.49	0.52	2.64	No
PlainGVF–Quadratic–Small	60	3.7	0.66	0.73	0.69	2.23	Yes
PlainGVF–Linear–Small	20	1.5	0.51	0.38	0.43	3.97	No
CannyGVF–Quadratic–Combined	(460)	(8.1)	0.89	0.78	0.83	0.69	Yes
CannyGVF–Linear–Combined	(340)	(5.3)	0.95	0.60	0.73	2.21	No
PlainGVF–Quadratic–Combined	(520)	(9.7)	0.91	0.78	0.84	0.75	Yes
PlainGVF–Linear–Combined	(300)	(5.1)	0.96	0.52	0.67	3.40	No

3.4. *Extraction of large-scale road networks*

The results of Experiment 4 are shown in Figure 11 and Table 8. The extracted road networks (Figure 11(c–f)) show the quadratic model's ability to capturing the detailed structure of a large-scale complex network. This can also be confirmed by comparing the Hausdorff distances reported in Table 8. Along the GVF type dimension, the Canny-based GVF provides more precise information on road edges than does the standard GVF. The relatively low precision of the quadratic models reported in Table 8 is due to the increased complexity of the road network and the snakes' failures to penetrate high-contrast image regions such as those containing buildings or small road loops. This large, complex road network consists of approximately 120 road segments and 70 intersections.

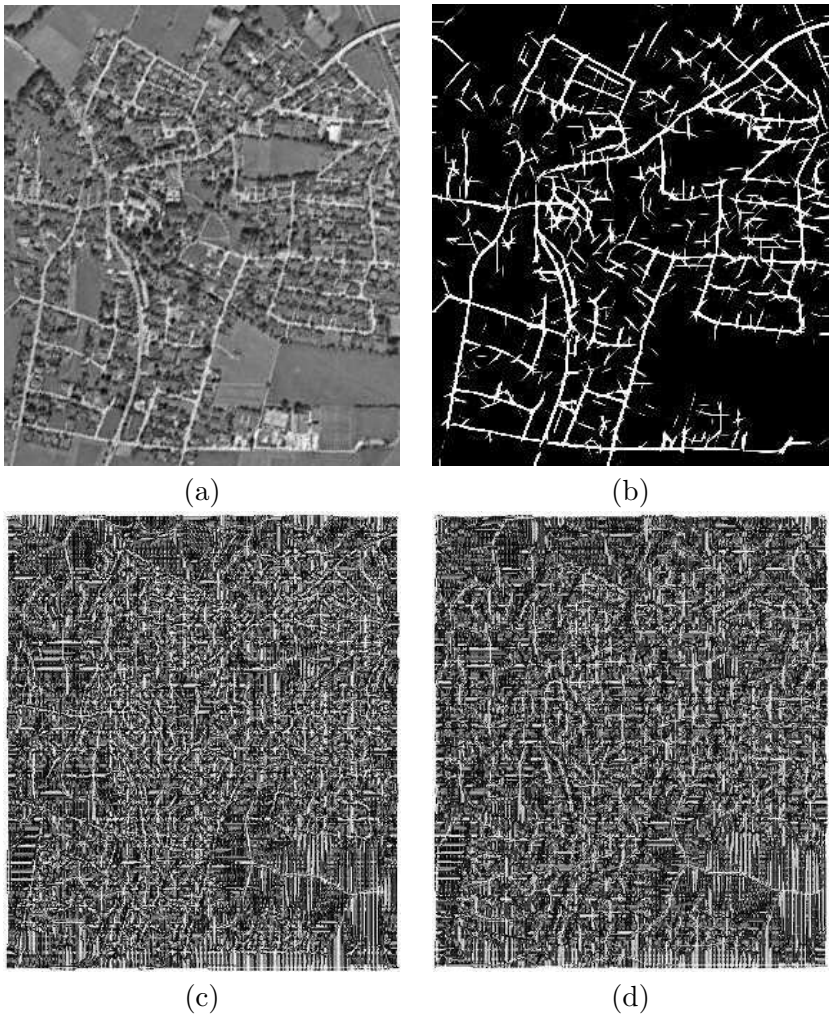

Figure 10. Experiment 4. (a) Original image, 277x322. (b) Oriented-filtered image. (c) Canny-based GVF. (d) Plain GVF.

Table 7. Parameters in Experiment 4.

Condition	σ_x	σ_y	α	β	λ	λ_{GVF}	d	ϵ
CannyGVF–Quadratic	1.3	7.2	0.02	0.48	40.0	0.32	1.08	0.73
CannyGVF–Linear	1.3	7.2	0.01	0	80.0	0.32	1.08	0.73
PlainGVF–Quadratic	1.3	7.2	0.02	0.48	40.0	0.32	1.08	0.73
PlainGVF–Linear	1.3	7.2	0.01	0	80.0	0.32	1.08	0.73

Table 8. Extraction results of Experiment 4.

Condition	Iterations	Time (s)	Precision	Recall	F_1	Averaged Hausdorff distance	Graph structure preserved
CannyGVF–Quadratic	950	299	0.56	0.51	0.53	2.27	Yes
CannyGVF–Linear	1000	146	0.51	0.47	0.49	4.43	No
PlainGVF–Quadratic	750	228	0.59	0.47	0.52	2.97	Yes
PlainGVF–Linear	1500	132	0.52	0.23	0.32	12.94	No

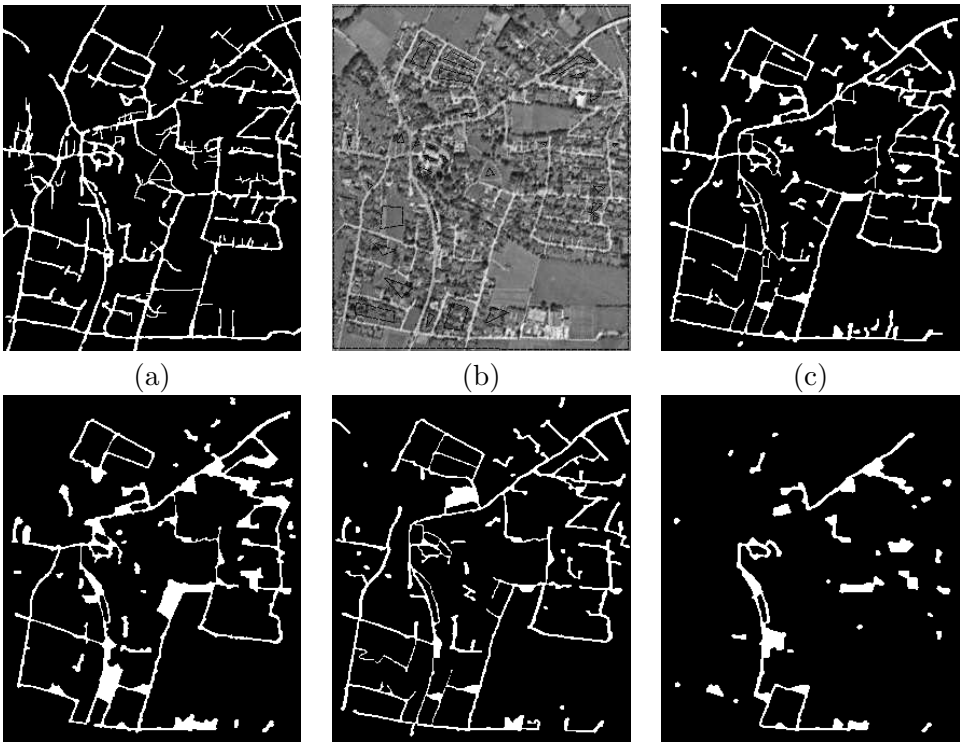

Figure 11. Experiment 4. (a) Ground truth. (b) Snake initialization. (c) Extraction with condition CannyGVF–Quadratic. (d) Extraction with condition CannyGVF–Linear. (e) Extraction with condition PlainGVF–Quadratic. (f) Extraction with condition PlainGVF–Linear.

4. Conclusion

In this paper, we have formulated a model for multiple interacting quadratic active contours and analyzed its performance in road network extraction on a test bed of satellite images, characterized by varying network complexity. The experiments demonstrate a clear advantage for multiple quadratic snakes, particularly in the case of complex road networks with multiple loops. In Experiment 1, the quadratic model is able to tolerate approximately 15 dB of noise. Over Experiments 2, 3, and 4, the accuracy of the quadratic models in terms of Hausdorff distance is 50%–80% better than the accuracy of the linear models. In terms of F_1, the quadratic models are 10%–40% better than the linear models. In Experiment 4, the linear snake's performance is clearly unacceptable, whereas the quadratic snakes perform quite well.

Our experiments also establish a performance improvement when the proposed quadratic model is coupled with the Canny-based GVF technique under circumstances. In Experiments 2, 3, and 4, the Canny-based GVF approach is 10%–25% better than the plain GVF approach in terms of Hausdorff although the F_1 measure itself does not indicate any significant performance improvement of the Canny-based GVF relative to the plain GVF.

Overall, in experiments 2, 3, and 4, we find that the quadratic snake model is capable of preserving the geometric structure of the road network, whereas the linear snake frequently fails to do so.

Given that our results approach the level of performance required by the GIS industry, the proposed model may eventually make automated extraction of road networks from satellite imagery practical. Future work will focus on computational optimization and automatic initialization of contours.

Acknowledgements

We wish to thank the anonymous referees of this paper for very useful comments and attention to details. This research is sponsored by *xxxxxx* (hidden due to double-blind review).

References

Auclair-Fortier, M.F., *et al.*, Survey of Work on Road Extraction in Aerial and Satellite Images. , 2000. , Technical report 247, Departement de mathematiques et d'informatique, Universitede Sherbrooke.

Barzohar, M. and Cooper, D., 1996. Automatic Finding of Main Roads in Aerial Images by Using Geometric-Stochastic Models and Estimation. *IEEE Transactions on Pattern Analysis and Machine Intelligence*, 18 (7), 707–721.

Caselles, V., *et al.*, 1993. A geometric model for active contours. *Numerische Mathematik*, 66, 1–31.

Choi, W., Lam, K., and Siu, W., 2001. An adaptive contour model for highly irregular boundaries. *Pattern Recognition*, 34 (2), 323–331.

Cohen, L.D., 1991. On active contour models and balloons. *CVGIP: Image Understanding*, 53 (2), 211–218.

Cohen, L.D. and Cohen, I., 1993. Finite-element methods for active contour models and balloons for 2-D and 3-D images. *IEEE Transactions on Pattern Analysis and Machine Intelligence*, 15 (11), 131–147.

Daugman, J.G., 1985. Uncertainty relation for resolution in space, spatial frequency, and orientation optimized by two-dimensional visual cortical filters. *Journal of the Optical Society of America A*, 2, 1160–1169.

Delingette, H. and Montagnat, J., 2000. New algorithms for controlling active contour shape and topology. *In*: *Sixth European Conference on Computer Vision (ECCV)*, Vol. 2, 381–395.

Durkovich, R., Kaneda, K., and Yamashita, H., 1995. Dynamic contour: A texture approach and contour operations. *Visual Computing*, 11, 227–289.

Fischler, M., Tenenbaum, J., and Wolf, H., 1981. Detection of Roads and Linear Structures in Low-Resolution Aerial Imagery Using a Multisource Knowledge Integration Technique. *Computer Graphics and Image Processing*, 15, 201–223.

Freeman, W. and Adelson, E., 1991. The design and use of steerable filters. *IEEE Transactions on Pattern Analysis and Machine Intelligence*, 13 (9), 891–906.

Fua, P. and Leclerc, Y., 1990. Model Driven Edge Detection. *Machine Vision and Applications*, 3, 45–56.

Geman, D. and Jedynak, B., 1996. An Active Testing Model for Tracking Roads in Satellite Images. *IEEE Transactions on Pattern Analysis and Machine Intelligence*, 18 (1), 1–14.

Giraldi, G., Strauss, E., and Oliveira, A., 2003. Dual-T-Snakes model for medical imaging segmentation. *Pattern Recognition Letters*, 24, 993–1003.

Heitger, F., *et al.*, 1992. Simulation of neural contour mechanisms: From simple to end-stopped cells. *Vision Research*, 32 (5), 963–981.

Ivins, J. and Porrill, J., 1995. Active region models for segmenting regions and colors. *Image and Vision Computing*, 13 (5), 431–438.

Ji, L. and Yan, H., 2002. Robust topology-adaptive snakes for image segmentation. *Image*

and Vision Computing, 20, 147–164.

Jones, J.P. and Palmer, L.A., 1987. An Evaluation of the Two-Dimensional Gabor Filter Model of Receptive Fields in Cat Striate Cortex. *Journal of Neurophysiology*, 58 (6), 1233–1258.

Kass, M., Witkin, A., and Terzopoulos, D., 1987. Snakes: Active contour models. *International Journal of Computer Vision*, 1 (4), 321–331.

Knutsson, H., Wilson, R., and Granlund, G., 1983. Anisotropic Nonstationary Image Estimation and its Applications: Part I — Restoration of Noisy Images. *IEEE Transactions on Communications*, COM-31 (3), 388–397.

Konishi, S., *et al.*, 2003. Statistical Edge Detection: Learning and Evaluating Edge Cues. *IEEE Transactions on Pattern Analysis and Machine Intelligence*, 25 (1), 57–74.

Li, C., Liu, J., and Fox, M., 2005. Segmentation of external force field for automatic initialization and splitting of snakes. *Pattern Recognition*, 38, 1947–1960.

Malladi, R., Sethian, J., and Vemuri, B., 1995. Shape modeling with front propagation: A level set approach. *IEEE Transactions on Pattern Analysis and Machine Intelligence*, 17, 158–175.

McInerney, T. and Terzopoulos, D., 2000. T-snakes: Topology adaptive snakes. *Medical Image Analysis*, 4 (2), 73–91.

Ngoi, K. and Jia, J., 1999. An active contour model for color region extraction in natural scenes. *Image and Vision Computing*, 17 (3), 955–966.

Perona, P. and Malik, J., 1990. Detecting and localizing edges composed of steps, peaks, and roofs. *In*: *International Conference on Computer Vision*, 52–57.

Regazzoni, C., Foresti, G., and Serpico, S., 1995. An adaptive probabilistic model for straight edge-extraction within a multilevel MRF framework. *In*: *International Geoscience and Remote Sensing Symposium*, 458–460.

Rochery, M., Jermyn, I.H., and Zerubia, J., 2006. Higher Order Active Contours. *International Journal of Computer Vision*, 69 (1), 27–42.

Samadani, R., 1989. Changes in connectivity in active contour models. *In*: *Proceedings of the Workshop on Vision Motion*, 337–343.

Sawano, H. and Okada, M., 2004. Road Extraction by Snake with Inertia and Differential Features. *In*: *International Conference on Pattern Recognition (ICPR)*, Vol. 4, 380–383.

Sethian, J., 1999. *Level Set Methods and Fast Marching Methods*. Cambridge: Cambridge University Press.

Steger, C., 1998. An unbiased detector of curvilinear structures. *IEEE Transactions on Pattern Analysis and Machine Intelligence*, 20 (2), 113–125.

Tang, J., 2009. A Multi-direction GVF Snake for the Segmentation of Skin Cancer Images. *Pattern Recognition*, 42 (6), 1172–1179.

Tang, J. and Acton, S., 2004. Vessel Boundary Tracking for Intravital Microscopy Via Multi–scale Gradient Vector Flow Snakes. *IEEE Transactions on Biomedical Engineering*, 51 (2), 316–324.

Tupin, F., *et al.*, 1998. Detection of Linear Features in SAR Images: Application to Road Network Extraction. *IEEE Transactions on Geoscience and Remote Sensing*, 36 (2), 434–453.

Wong, Y., Yuen, P., and Tong, C., 1998. Segmented snake for contour detection. *Pattern Recognition*, 31 (11), 1669–1679.

Xu, C., Pham, D., and Prince, J., 2000. *Image segmentation using deformable models*. SPIE Press.

Xu, C. and Prince, J.L., 1997. Gradient Vector Flow: A New External Force for Snakes.

In: *IEEE Conference on Computer Vision and Pattern Recognition (CVPR)*, 66–71.

Xu, C. and Prince, J., 1998a. Generalized gradient vector flow external forces for active contours. *Signal Processing*, 71 (2), 131–139.

Xu, C. and Prince, J., 1998b. Snakes, Shapes, and Gradient Vector Flow. *IEEE Transactions on Image Processing*, 7 (3), 359–369.